Journal of Power Sources 513 (2021) 230543

Contents lists available at ScienceDirect

Journal of Power Sources

journal homepage: www.elsevier.com/locate/jpowsour

1D $NiHPO_4$ nanotubes prepared using dissolution equilibrium as bifunctional electrocatalyst for high-efficiency water splitting

Zining Wang [a,1], Yutai Wu [a,1], Mengqi Cui [a], Shan Ji [b,*], Hui Wang [a], Xuyun Wang [a], Valdimir Linkov [c], Rongfang Wang [a,**]

[a] State Key Laboratory Base for Eco-Chemical Engineering, College of Chemical Engineering, Qingdao University of Science and Technology, Qingdao, 266042, China
[b] College of Biological, Chemical Science and Chemical Engineering, Jiaxing University, Jiaxing, 314001, China
[c] South African Institute for Advanced Material Chemistry, University of the Western Cape, Cape Town, 7535, South Africa

HIGHLIGHTS

- Ni foam-supported $NiHPO_4$ nanotubes catalyst is prepared without any template.
- The mechanism of evolving $NiHPO_4$ nanotubes based on dissolution equilibrium is proposed.
- $NiHPO_4$ nanotubes shows good bifunctional performance for overall water solitting
- The present work provides a strategy to explore efficient electrocatalysts.

GRAPHICAL ABSTRACT

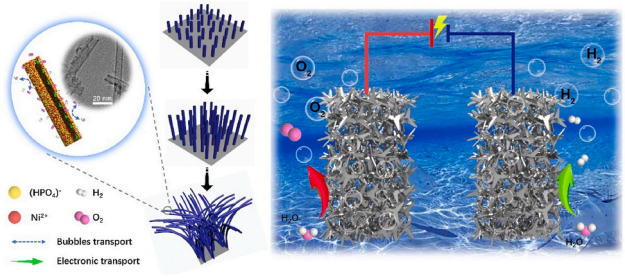

ARTICLE INFO

Keywords:
Dissolution equilibrium
Solvent effect
Hollow structure
$NiHPO_4$ nanotubes
Water splitting

ABSTRACT

In this work, one-dimensional $NiHPO_4$ nanotubes are successfully fabricated on nickel foam by hydrothermal reaction, in which a dissolution equilibrium between phosphates is controlled by tuning the proportion of the mixed solvent and amounts of KOH. As the dissolution equilibrium is broken, the morphology of $NiHPO_4$ transfers from solid nanowires to hollow nanotubes. The resulting 1D $NiHPO_4$ nanotubes exhibit good electrocatalytic activity and stability in oxygen evolution reaction (OER) and hydrogen evolution reaction (HER). Notably, a water-splitting voltage of 1.62 V at a current density of 10 mA cm^{-2} is obtained in an electrolyzer setup assembled using 1D $NiHPO_4$ nanotubes as cathode and anode, demonstrating $NiHPO_4$ nanotubes are promising catalysts for overall water splitting. Moreover, the revealed mechanism of forming tube morphology can be extended to fabricate other metal phosphates with hollow structures.

1. Introduction

The global energy crisis and environmental pollution have been stimulating the development of sustainable energy conversion and storage technologies [1,2]. Hydrogen is now regarded as a promising alternative energy carrier to replace fossil fuels because it can be

* Corresponding author.
** Corresponding author.
E-mail addresses: jishan@mail.zjxu.edu.cn (S. Ji), rfwang@qust.edu.cn (R. Wang).
[1] These authors contributed equally to this work and are regarded as co-first authors.

https://doi.org/10.1016/j.jpowsour.2021.230543
Received 1 July 2021; Received in revised form 1 September 2021; Accepted 16 September 2021
Available online 24 September 2021

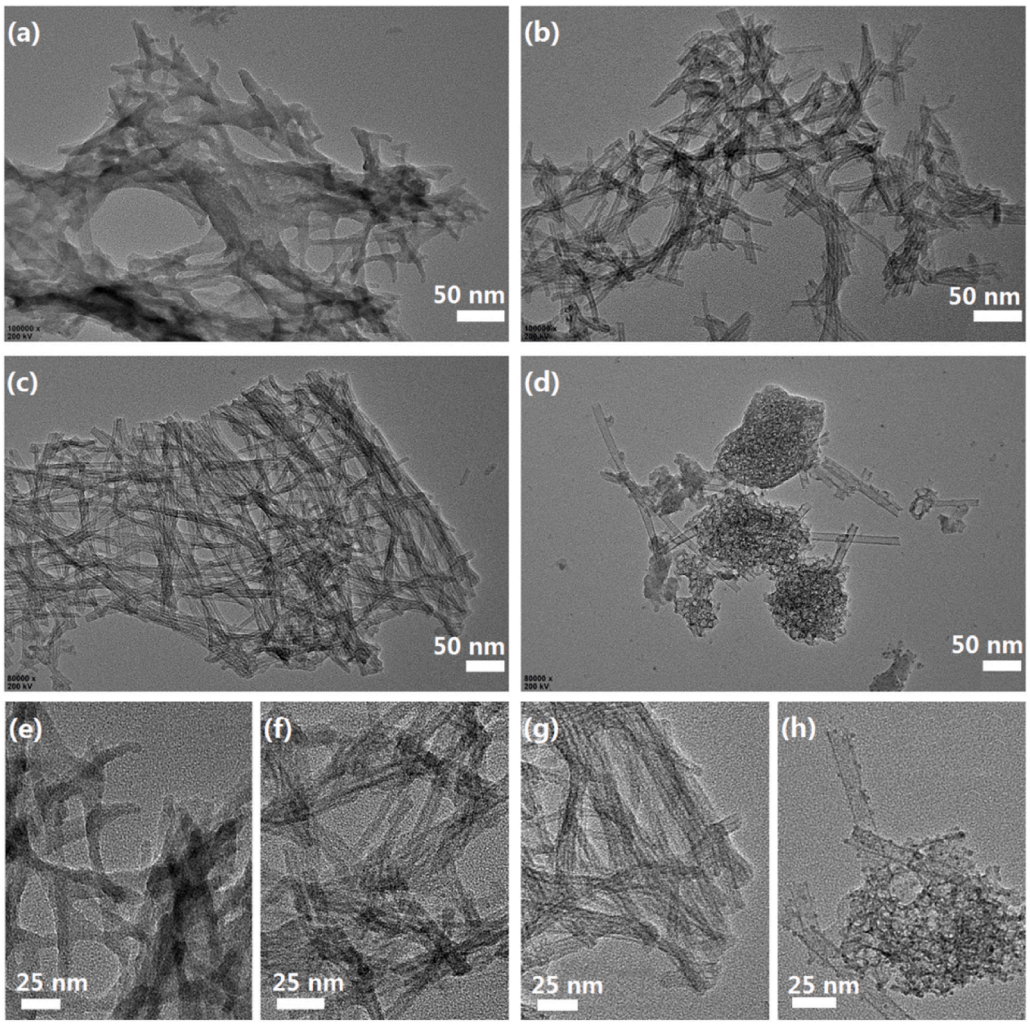

Fig. 1. Effects of the amounts of KOH on the morphology of $NiHPO_4$, (a, e) without KOH; (b, f) 0.5 mL KOH; (c, g) 1 mL KOH; (d, h) 5 mL KOH.

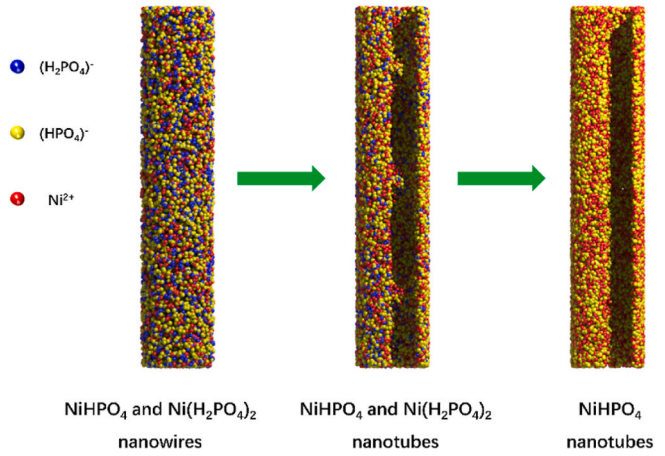

Fig. 2. Schematic diagram of transformation from nanowire to nanotube based on solution equilibrium.

produced by water splitting using excess solar or wind energy. In a water electrolyzer, oxygen evolution reaction (OER) occurs on the anode and hydrogen evolution reaction (HER) on the cathode. Both reactions are occurring in the presence of platinum group metals (PGM) containing electrocatalysts, such as Pt/C for HER, and IrO_2 and RuO_2 for OER, which reduce the reactions' over-potentials resulting in higher energy conversion efficiency of electorlysers [3–5]. However, high costs and scarcity of PGM based catalysts significantly impede large scale applications of water electrolysis. Additionally, HER and OER electrocatalysts usually work well in different electrolytes, resulting in low overall efficiency of water electrolysis cells where both cathode and anode are immersed in the same electrolyte [6–8]. Therefore, there is a high demand for bifunctional HER and OER electrocatalysts based on abundant chemical elements to achieve wider adoption of hydrogen generation using water electrolysis.

Many nano-sized transition metal-based materials, such as oxides [9,10], phosphides [11,12], sulfides [13], nitrides [14,15] and carbides [16,17] have been developed as HER and OER catalysts for water splitting due to their high intrinsic activity and low cost. Recently, transition metal phosphates were added to this group of materials due to their low cost, good electrical conductivity and electrocatalytic performance, which promise significant application potential in electrochemical technologies. Rapid development of nanotechnology and nanostructure engineering provides promising ways to maximize electrocatalytic performance of electrode materials for large-scale applications in renewable and green energy systems. It was reported that charge accumulation and redox reactions can be efficiently improved using one-dimensional (1D) materials, especially 1D nanotubes, due to the space-confined transport phenomena [18,19]. Additionally, the unique hollow structure of 1D nanotubes offers the advantages of high surface area, high porosity and internal void space, providing a large number of

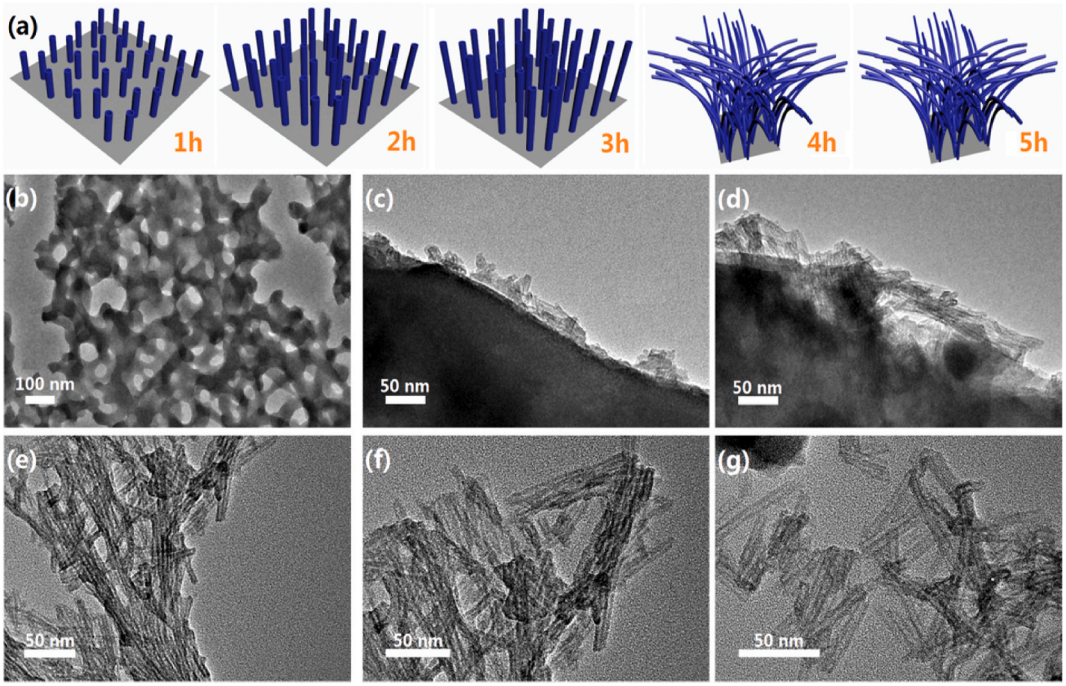

Fig. 3. Effects of different reaction times on phosphate structure, (a) $NiHPO_4$ growth illustration at different heating times; TEM images of the samples after (b) reacted at room temperature for 0.5 h; (c) heated for 1 h; (d) heated for 2 h; (e) heated for 3 h; (f) heated for 4 h; (g) heated for 5 h (all samples shown in Fig. 3c–g were heated at 160 °C).

accessible active sites for surface charge storage and catalytic reactions [20–22]. Moreover, their thin shells could relax structural strains associated with ion insertion [23]. Due to these advantages, 1D nanotubes have become an active research topic in chemical catalysis, biomedical engineering, energy storage and conversion [24]. For instance, 1D hollow structured NiCoP nanowires were synthesized directly on Ni foam using the Kirkendall Effect, and the obtained NiCoP nanowires exhibited low onset potential with superior stability in HER [25]. 1D microrods of NH_4NiPO_4 were prepared by Ozoemena et al. as an electrode material for pseudocapacitors with high energy rating and power handling [18]. Self-templated techniques to prepare hollow nanostructures are also widely reported, among them processes using hard or soft templates [24,26–28], advanced selective etching [29,30], outward diffusion [31,32] and heterogenous contraction [33,34]. Although 1D materials show many advantages, their harsh and strictly controlled synthesis conditions still restrict large scale applications, which require the development of easily controllable synthesis routes utilizing abundant resources. Fabricating hollow nanostructures without using any template gained much research attention recently due to simple synthetic procedures and controllable morphology of resulting products. Hollow structures which are made of crystals or noncrystals can be fabricated via the dissolution regrowth process, which, unlike Ostwald ripening, doesn't happen spontaneously, but requires additional chemical to etch the solid particle precusors. During the dissolution regrowth process, the dissoluble precursor redeposits on the surface and results in the formation of hollow structure [23,35].

In this work, motivated by the advantages of transition metal phosphates and 1D nanotubes, we designed and synthesized 1D $NiHPO_4$ nanotubes using different solubilities of $Ni(H_2PO_4)_2$ and $NiHPO_4$. This was carried out by moderate alteration of the solvent pH to break original hydrolysis balance of $H_2PO_4^-$, and simultaneously synthesize Ni $(H_2PO_4)_2$ and $NiHPO_4$. An investigation into the relationship between the structure of 1D $NiHPO_4$ nanotubes and their catalytic performance in HER and OER revealed significant improvements in both electrochemical activity and stability. Seldomly reported synthesis of 1D $NiHPO_4$ nanotubes by controlling the dissolution equilibrium provides a promising route for the preparation of electrocatalytically active hollow nanomaterials.

2. Experiment

Synthesis of $NiHPO_4$ nanotubes. All chemicals used in the study were of analytical grade and utilized directly without further purification. Initially, nickel foam (2 cm × 3 cm) was immersed in a 1.0 M aqueous HCl solution, followed by sonication for 20 min. The acid-treated nickel was washed alternately with ethanol and deionized water, and dried in a vacuum oven at 60 °C. 5 mmol of NaH_2PO_4 was dissolved in 25 mL of ultrapure water, followed by the addition of 0.5–10 mL 1 M KOH solutions. After the addition of 25 mL 1 mM Ni $(NO_3)_2$ ethanol solution and careful placement of the treated Ni foam at their bottom, the containers with NaH_2PO_4 were transferred into a Teflon-lined autoclave and heated at 160 °C for 1–5 h. The obtained Ni foam was rinsed by ethanol and water and vacuum dried at 40 °C for 12 h.

Reaction equations with adding 0.5, 1.0 mL KOH are as follows:

$$OH^- + H_2PO_4^- \rightleftharpoons HPO_4^{2-} + H_2O \quad (1)$$

$$Ni^{2+} + HPO_4^{2-} \rightleftharpoons NiHPO_4 \quad (2)$$

$$Ni^{2+} + 2H_2PO_4^- \rightleftharpoons Ni(H_2PO_4)_2 \quad (3)$$

An appropriate amount of KOH was added to break the original dissolution equilibrium of NaH_2PO_4 and the hollow structure would form during this process. The details of physical characterization and electrochemical measurements of the synthesized materials are described in the Supporting Information section.

3. Results and discussion

3.1. Synthesis mechanism of 1D $NiHPO_4$ nanotubes

Solvent effect. Composition and the solubility of the phosphate are

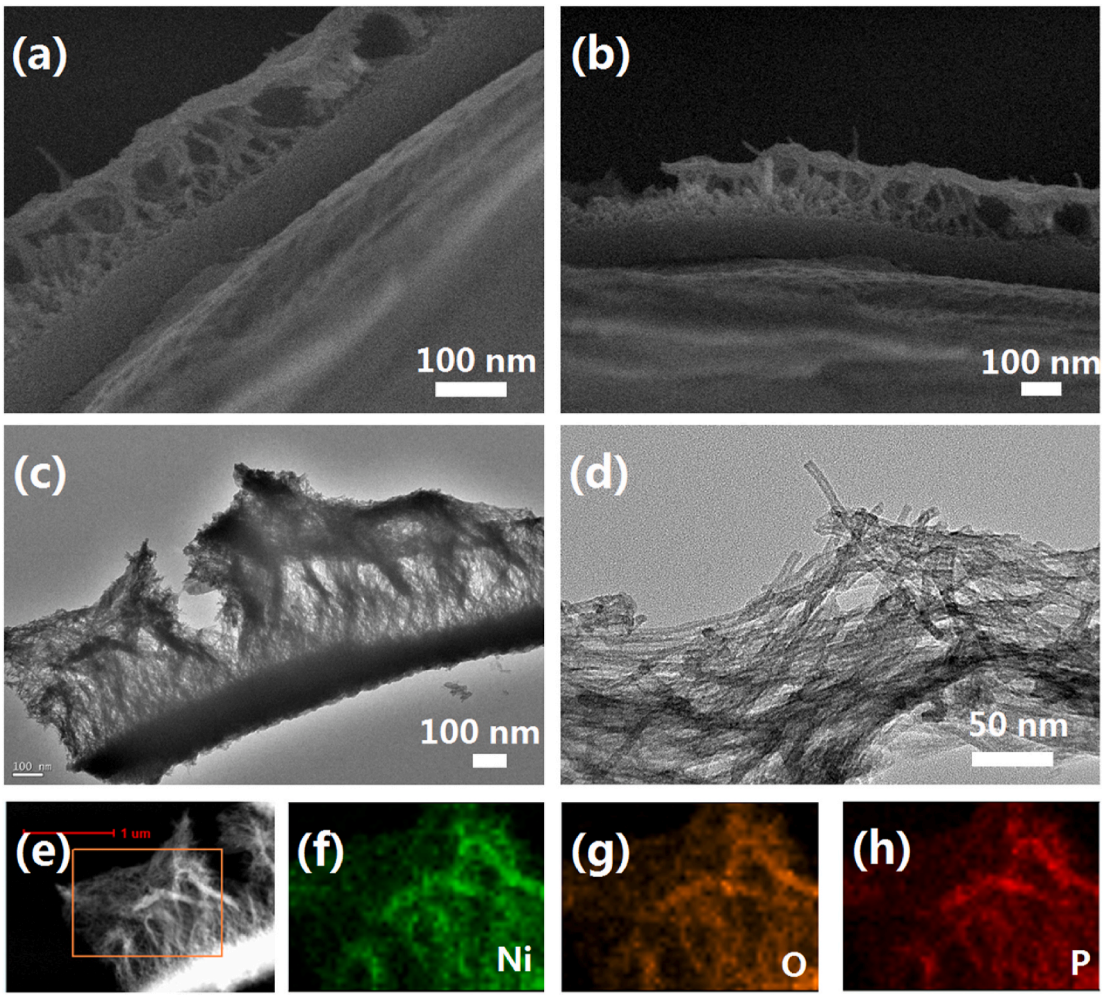

Fig. 4. (a, b) SEM images of $NiHPO_4$ layer on Ni foam; (c, d) TEM images of $NiHPO_4$ on Ni foam; (e) STEM image; (f–h) STEM-EDS element maps of Ni, O and P.

affected by the solvents, then, the effect of the solvent in the $NiHPO_4$ synthesis process was firstly investigated. As shown in Figs. S1(a and b), the obtained $NiHPO_4$ consisted of irregular large particles, when only water was used as a solvent during the hydrothermal synthesis. When a mixed solvent containing ethanol and water at a volume ratio of 1:1 was used, a uniform hair-like structure was evenly formed on Ni foam (Figs. S1(c and d)). No $NiHPO_4$ was detected on Ni foam when only ethanol was used, due to very low precursor solubility in this solvent (Figs. S1(e and f)). These phenomena suggest the composition of the solvents play an important role in the formation of $NiHPO_4$ nanotubes, in agreement with the previously reported effect of polarity and solubility of solvents on the nucleation and crystal growth of transition-metal-based nanostructures with the possibility of fine-tuning materials' morphology [36].

Similarly, the solvent pH value, determined by KOH concentration, plays a critical role in the type of $NiHPO_4$ final structure formed. Separate addition of 0, 0.5, 1.0, 5.0, and 10.0 mL of 1 M KOH into ethanol/water mixed solvent with a volume ratio of 1:1, resulted in the preparation of three different materials, such as $Ni(H_2PO_4)_2$ (without and 0.5 mL KOH), $NiHPO_4$ (1.0 and 5.0 mL KOH) and $Ni_3(PO_4)_2$ (10.0 mL KOH). It can be seen from Figs. S2 and S3 that only solid nanowires originated from the synthesis solutions without KOH addition (Fig. 1(a, e)) and nanotubes were formed in the solutions containing 0.5 mL (Fig. 1 (b, f)) and 1.0 mL of KOH (Fig. 1(c,g)). The results indicated the morphology of the products was affected by the solvent pH value.

3.2. Dissolution equilibrium process

The above results show that the composition and pH of the solvents play important role in the final structure formed, it could be assumed that the nanotube growth process included several stages, starting with the loss of the hydrolysis balance of $H_2PO_4^-$ in ethanol and water mixed solvent at a high pH, resulting in the formation of a supersaturated amorphous phase, rapid nucleation and instantaneous precipitation of mutually converting $Ni(H_2PO_4)_2$ and $NiHPO_4$ in the form of stable particles [35]. The conversion of nanowires to nanotubes due to different solubilities of $Ni(H_2PO_4)_2$ and $NiHPO_4$ is illustrated in Fig. 2. Dissolution and transformation of $Ni(H_2PO_4)_2$ leads to the outward diffusion of $NiHPO_4$ accompanied by voids growth inside the nanowires and its surface re-deposition to produce stable $NiHPO_4$ nanotubes [35]. No hollow structured nanotubes were observed in corresponding SEM images presented in Fig. S3. when a high quantity of KOH was added to the reaction mixture, indicating that nanotubes can only be obtained at a certain pH range allowing for conversion reactions between $Ni(H_2PO_4)_2$ and $NiHPO_4$ to take place. Possible reactions occurring at different amounts of KOH values are proposed in the Supporting Information section.

According to TEM and SEM study of the effect of heating time on the nanotube morphology presented in Figs. 3(b) and S4, only very short and solid nanowires resulted from a 30 min reaction at a room temperature. Heating the reaction mixture at 160 °C for 1 h produced even nanostructured coating, thin enough for Ni foam to be visible in SEM images (Fig. S5). The corresponding TEM image reveals short surface

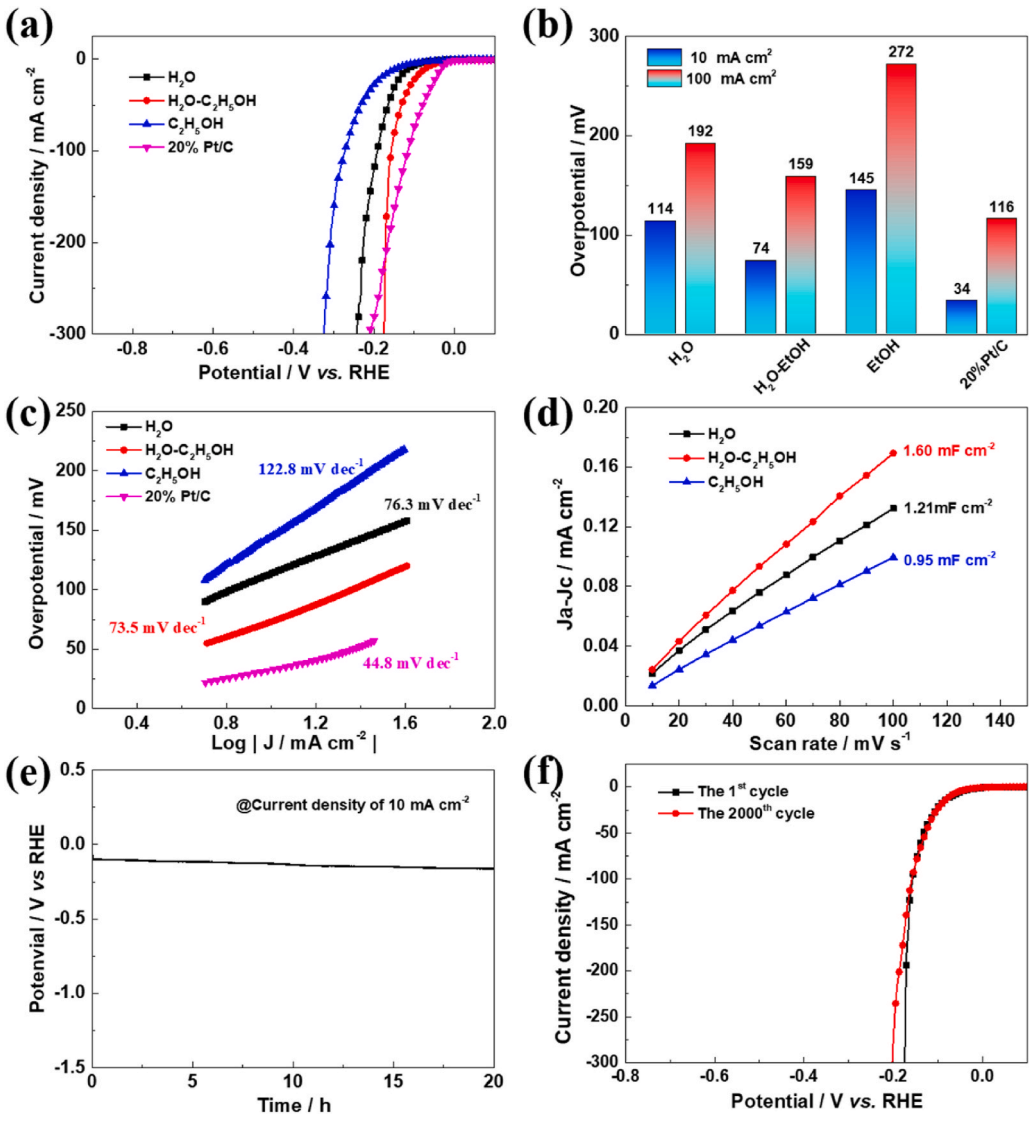

Fig. 5. HER electrocatalytic measurements in 1.0 M KOH: (a) linear sweep voltammogram (LSV); (b) overpotentials comparison for all samples at $j = 10$ and 100 mA cm^{-2}; (c) Tafel plots; (d) electrochemical double-layer capacitances; (e) chronopotentiometry of HER at 10 mA cm^{-2}; (f) HER LSV curves of 1st and 2,000th cycles.

nanotubes whose hollow structure was formed during 1h (Fig. 3(c)). According to Fig. S6, the surface of Ni foam was fully and evenly covered by hair-like nanomaterials when the heating time was further increased to 2 h, and the thickness of the coating increased substantially (Fig. 3 (d)). As the heating time continued to increase, the nanowires gradually grew longer, as shown in Figures S7-8 and 3(e-g). All samples coated during extended periods of time contained nanotubes, as per TEM images (Fig. 3(e–g)), with no structural differences visible for coating times up to 4 h, at which point the process of $NiHPO_4$ nanotubes formation appeared to be completed.

3.3. Characterization of 1D $NiHPO_4$ nanotubes

The morphology of as-prepared $NiHPO_4$ coating on the surface of Ni foam was initially investigated by scanning electron microscopy (SEM) which demonstrated a uniform layer with a thickness of ca. 300 nm (Figs. 4(a) and 1(b)). Hair-like structures in the form of thin and dense wires grown vertically on Ni foam are visible in Fig. 4(c). A zoom-in TEM images shown in Figs. 4(d) and S9 reveal that the hair-like layer consisted of straight and long wires with hollow structures of similar diameters, representing a nanotube morphology. No other growths were observed in the TEM image, indicating that uniform $NiHPO_4$ nanotubes were formed on Ni foam by the hydrothermal method developed in this study. The scanning transmission electron microscopy (STEM) image and the elemental mapping shown in Fig. 1(f–h) demonstrate even distribution of Ni, O and P elements in the nanotubes, further confirming chemical composition of $NiHPO_4$.

Crystallinity of as-prepared $NiHPO_4$ was analyzed by X-ray diffraction (XRD) as shown in Fig. S10(a). Characteristic peaks of pure Ni at 44.5°, 51.8° and 76.3°, corresponding to (111), (200) and (220) planes respectively (PDF#04-0805), are clearly visible in the XRD pattern of $NiHPO_4$. The major characteristic peaks shown in the standard XRD pattern of $NiHPO_4$ (PDF#39-0706) are well matched with the XRD pattern of the newly prepared material. Besides the diffraction peaks of Ni and $NiHPO_4$, no other peaks were observed in Fig. S10(a), confirming that only $NiHPO_4$ compound was formed on Ni foam. Chemical composition of $NiHPO_4$ was further evaluated by X-ray photoelectron spectroscopy (XPS) as Fig. S10(b), where a high-resolution Ni 2p spectrum, with two main peaks, corresponding to Ni $2p_{3/2}$ (854.6 eV) and Ni $2p_{1/2}$ (872.4 eV), accompanied by two satellite vibration peaks, is shown. Ni $2p$ XPS spectrum exhibits a typical feature of Ni^{2+} bonded with oxygen [37,38]. The fitted high-resolution P 2p XPS spectrum shows two peaks at 134.0 and 133.1 eV, ascribed to P $2p_{3/2}$ and P $2p_{1/2}$, due to the oxidized phosphorous species of HPO_4^{2-} (Fig. S10(c)) [39].

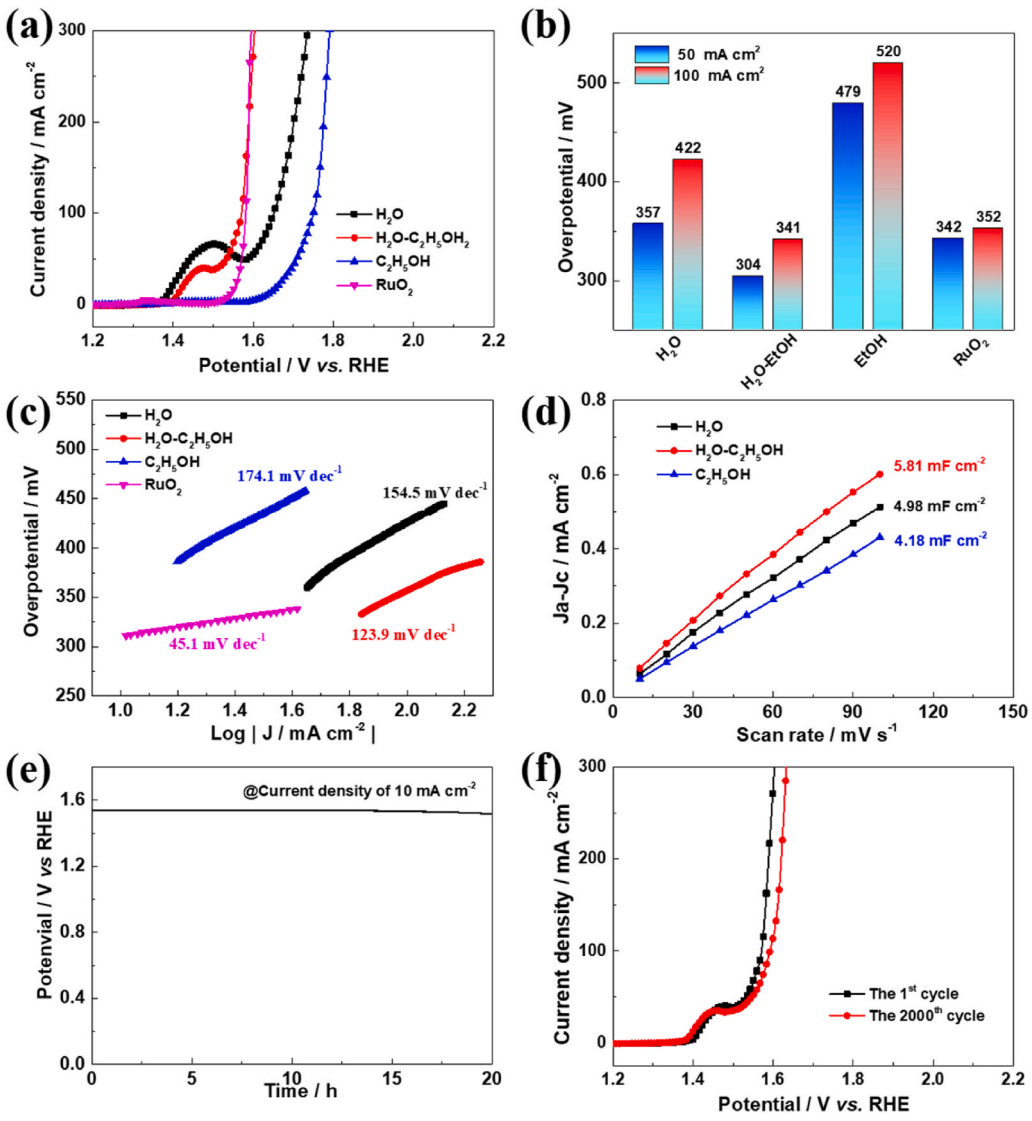

Fig. 6. OER electrocatalytic measurements in 1.0 M KOH: (a) Linear sweep voltammogram (LSV); (b) corresponding overpotentials at j = 10, 100 mA cm^{-2} respectively; (c) Tafel plots; (d) electrochemical double-layer capacitances for the samples; (e) chronopotentiometry measurements of OER at 10 mA cm^{-2}; (f) OER LSV curves for the 1st and 2,000th cycles of the $NiHPO_4$ nanotubes.

Fig. S10 (d) shows a peak at 529.2 eV corresponding to O 1s, indicating that plenty of oxygen was bonded with P [40] and further confirming the formation of $NiHPO_4$.

3.4. Electrochemical performances of 1D $NiHPO_4$ nanotubes

Electrochemical properties of $NiHPO_4$ samples prepared in different solvents were initially evaluated using HER in a 1.0 M KOH electrolyte and benchmarked against the state-of-the-art HER catalyst, Pt/C (20%). As shown in Fig. 5(a), all as-prepared $NiHPO_4$ samples demonstrated quite high HER activity. Specifically, the $NiHPO_4$ sample prepared in water and ethanol has a low onset potential of ca. −23 mV at a current density of 10 mA cm^{-2} (Fig. 5(b)). Although its onset potential was higher than that of Pt/C, the cathode current on $NiHPO_4$ increased much faster at higher biases, indicating superior electrochemical activity towards HER [41]. The activity of the catalysts was also normalized by the specific surface area, and the BET surface area was obtained from the nitrogen physisorption provided in Fig. S11. The obtained BET surface area of the samples with adding 0, 0.5, 1, 5, 10 mL were 3.85, 4.71, 5.25, 3.37 and 3.22 m^2 g^{-1} respectively. The difference of these obtained BET surface areas is quite minimal. This is because nickel foam is the main part of all the measured samples, and the amount of nickel foam in all the samples is similar. As shown in Fig. S12, the specific activity order of these samples is similar to that of figures presented in Fig. 5(a), in which the current was normalized by the geometric surface area, suggesting the enhanced electrochemical performance is a result of enhanced inherent properties of the catalysts.

Tafel plots were used to further investigate electrochemical properties $NiHPO_4$ nanotube-coated materials, as shown in Fig. 5(c) where the sample prepared in H_2O–C_2H_5OH has the smallest Tafel value of 73.5 mV dec^{-1}, indicating favorable HER reaction kinetics. Cyclic voltammetry (CV) performed in the potential range with no Faradic current (Fig. S13), was instrumental in the evaluation of electrochemical double-layer capacitance, an indication of HER effective surface area, as illustrated in Fig. 5(d), where $NiHPO_4$ nanomaterial prepared in H_2O–C_2H_5OH solution exhibited the highest values among the three samples.

HER stability of $NiHPO_4$ containing bifunctional electrocatalysts, which is critical for their intended water splitting application, was investigated by chronopotentiometry and linear sweep voltammetry (LSV). According to Fig. 5(e), the overpotential of $NiHPO_4$ (H_2O–C_2H_5OH) was initially −74 mV and only dropped by 0.5 mV after

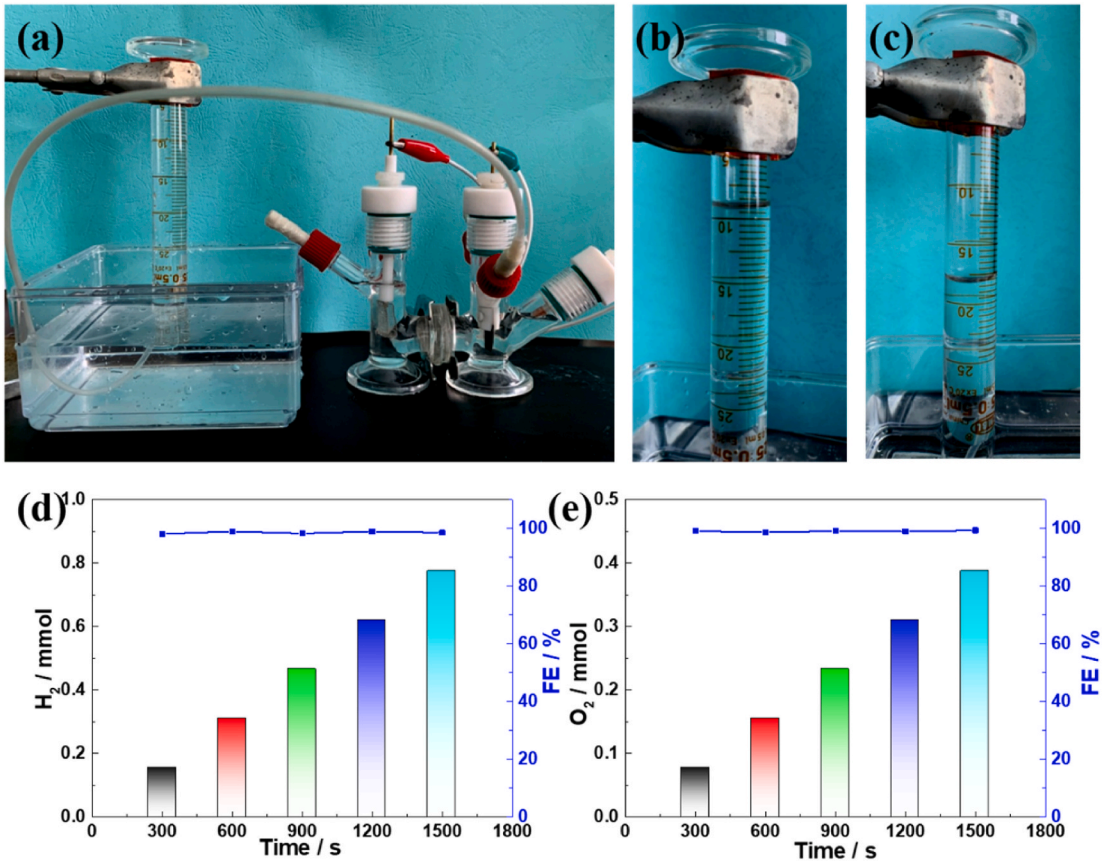

Fig. 7. (a) Three-electrode configuration for gas collection; (b, c) O_2 and H_2 gas volumes collected; (d, e) gas generation rates and corresponding Faradaic efficiencies.

20h of operation at a current density of 10 mA cm^{-2}, indicating its good stability under HER conditions. This was further confirmed by LSV plots of 1st and 2000th cycles almost overlapping with each other at current densities lower than 100 mA cm^{-2} (Fig. 5(f)). It was also shown that the addition of 1 mL KOH into the $NiHPO_4$ synthesis mixture resulted in the material with best HER performance among all samples (Figs. S11–15).

The activity of newly prepared catalytic materials toward OER was evaluated in oxygen-saturated KOH electrolyte and compared with that of the state-of-the-art RuO_2 electrocatalyst, which similar performance is illustrated in Fig. 6(a) normalized by the geometric surface area and in Fig. S16 normalized by the specific surface area. While OER overpotentials of $NiHPO_4$ (H_2O–C_2H_5OH) at 50 and 100 mA cm^{-2} were even lower than those of RuO_2, as shown in Fig. 6(b), $NiHPO_4$ materials prepared using other solvents were significantly less electrocatalytically active.

Tafel plots were used to study OER kinetics as shown in Fig. 6(c) where, at 123.9 mV dec^{-1}, the Tafel slope value of $NiHPO_4$ (H_2O–C_2H_5OH) is was much higher than those of $NiHPO_4$ prepared in water or ethanol, indicating critical role of nanotubular surface morphology in OER activity of this bifunctional electrocatalyst [31]. This was further confirmed by the evaluation of OER effective surface area using electrochemical double-layer capacitor as shown in Figs. 6(d) and S17. Again, at 5.81 mF cm^{-2}, the capacitance of $NiHPO_4$ (H_2O–C_2H_5OH) was higher than that of other two samples, indicating abundant electrocatalytically active sites available on its surface.

High stability of $NiHPO_4$ (H_2O–C_2H_5OH) under OER conditions was demonstrated by chronopotentiometry and linear sweep voltammetry as shown in Fig. 6(e–f) where, at a current density of 10 mA cm^{-2}, the overpotential decreased by only 30 mV after 20 h operation and shifted positively by 15 mV after 2000 continuous CV cycles. The OER performance investigation was augmented by establishing the optimal quantity of KOH to be added to the electrocatalyst synthesis mixture, which, according to Figs. S17–19, was 1 mL.

The gas collection electrolysis system shown in Fig. 7(a–c) was used to evaluate the overall water splitting activity of the newly prepared electrocatalyst under more practical conditions. H_2 and O_2 generation were continuously observed at a 2:1 vol ratio (Fig. 7(b and c)) with 0.77 mmol hydrogen collected in about 1500 s, corresponding to hydrogen yield of 1.85 mmol h^{-1}, and Faraday efficiency (FE) close to 98.5% (Fig. 7(d)). 0.38 mmol oxygen was collected at the same time at an oxygen production rate of 0.94 mmol h^{-1} and FE close to 98.9% (Fig. 7 (e)) [42].

Finally, overall water splitting performance of $NiHPO_4$ nanotube as bifunctional HER and OER electrocatalyst was evaluated under real-world conditions in a two-electrode cell. A current density of 10 mA cm^{-2} was achieved at 1.62 V, which was only slightly higher than 1.56 V required to reach the same current density in Pt/C||RuO_2 containing electrolyzer setup (Fig. 8(a–c)). The stable performance of $NiHPO_4$ electrocatalyst is demonstrated in Fig. 8(d) where 40 h operation of the electrolyzer at 10 mA cm^{-2} resulted in a cell voltage increase of only 70 mV, with plenty of gas bubbles evolving on both electrodes as per the insert picture. The performance comparison between $NiHPO_4$ nanotube electrocatalyst and previously reported Ni based water splitting equivalents, presented in Table S3, clearly demonstrates the advantages of the newly developed material.

The applicability of the obtained $NiHPO_4$ as anode and cathode in anion exchange membrane water electrolysis (AEMWE), a membrane electrode assembly (MEA) coated with $NiHPO_4$ were prepared [43,44]. For comparison, the MEA coated with Pt/C and RuO_2 was also fabricated. At the current density of 100 mA cm^{-2}, the cell voltage of $NiHPO_4$ AEMWE cell is 1.94V, with an energy conversion efficiency of 68%, which is close to that of RuO_2 and Pt/C cell. As shown in Table S4, the

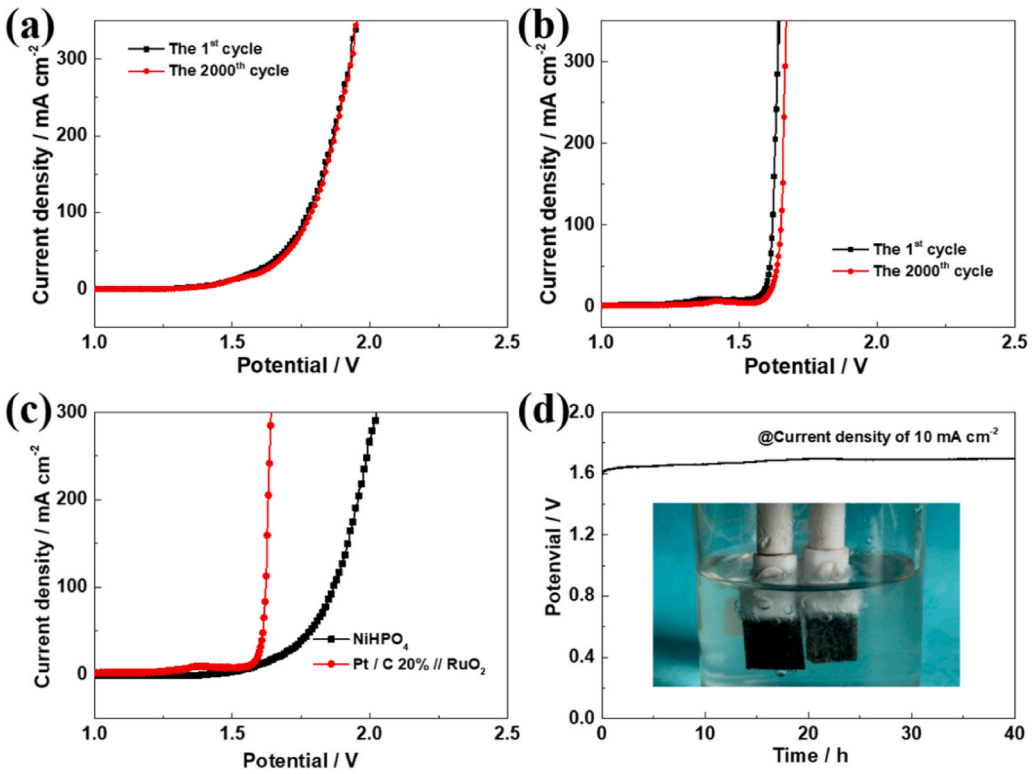

Fig. 8. (a,b) Polarization curves of the $NiHPO_4$ nanotubes electrolyzer (b) and Pt/C||RuO_2 (b) for overall water splitting at the 1st and 2,000th cycles; (c) polarization curves of $NiHPO_4$ nanotube electrocatalyst for overall water splitting; (d) chronopotentiometry analysis in two-electrode configuration at constant current density of 10 mA cm^{-2}.

electrocatalytic performance of $NiHPO_4$ AEMWE cell is on par with many other representative transitional-metal-based materials reported previously.

4. Conclusions

In this study, an effective dissolution equilibrium method based on the hydrothermal process was developed to prepare 1D $NiPHO_4$ nanotubes on Ni mesh. It was found that the formation of 1D $NiPHO_4$ nanotubes involved in an evolution process from nanoparticle nucleus, solid $Ni(H_2PO_4)_2$ nanofibres to $NiHPO_4$ nanotubes as a result of breaking the original $H_2PO_4^-$ and HPO_4^- dissolution equilibrium. Using 1D $NiHPO_4$ nanotube material as both a cathode and an anode in an electrolyzer, a current density of 10 mA cm^{-2} could be obtained at 1.62 V, which was attributed to the abundance of active surface sites and enhanced ion transfer properties. Moreover, the $NiHPO_4$ AEMWE cell also exhibited outstanding performance in 1 M KOH at 25 °C. With high catalytic activity and stability of 1D $NiHPO_4$ nanotubes grown on Ni foam, this study provides a promising template-free synthesis route towards hollow nanomaterials.

CRediT authorship contribution statement

Zining Wang: Methodology, Validation, Writing – original draft. **Yutai Wu:** Validation, Writing – original draft. **Mengqi Cui:** Formal analysis. **Shan Ji:** Conceptualization, Resources, Writing – review & editing. **Hui Wang:** Methodology, Validation, Writing – original draft. **Xuyun Wang:** Visualization. **Valdimir Linkov:** Writing – review & editing. **Rongfang Wang:** Conceptualization, Resources, Supervision.

Declaration of competing interest

The authors declare that they have no known competing financial interests or personal relationships that could have appeared to influence the work reported in this paper.

Acknowledgments

The authors would like to thank the National Natural Science Foundation of China (21766032), the Key Research and Development Program of Shandong Province of China (2019GGX103029) and the Natural Science Foundation of Shandong Province of China (ZR2020MB024) for financially supporting this work.

Appendix A. Supplementary data

Supplementary data to this article can be found online at https://doi.org/10.1016/j.jpowsour.2021.230543.

References

[1] P. Menezes, C. Panda, S. Loos, F. Bruns, C. Walter, M. Schwarze, X. Deng, H. Dau, M. Driess, A structurally versatile nickel phosphite acting as a robust bifunctional electrocatalyst for overall water splitting, Energy Environ. Sci. 11 (2018) 1287–1298.
[2] H. Sun, Z. Yan, F. Liu, W. Xu, F. Cheng, J. Chen, Self-supported transition-metal-based electrocatalysts for hydrogen and oxygen evolution, Adv. Mater. 32 (2019) 1806326.
[3] S. Anantharaj, S. Ede, K. Sakthikumar, K. Karthick, S. Mishra, S. Kundu, Recent trends and perspectives in electrochemical water splitting with an emphasis on sulfide, selenide, and phosphide catalysts of Fe, Co, and Ni: a review, ACS Catal. 6 (2016) 8069–8097.
[4] J. Joo, T. Kim, J. Lee, S. Choi, K. Lee, Morphology-controlled metal sulfides and phosphides for electrochemical water splitting, Adv. Mater. 31 (2019) 1806682.
[5] Z. Wang, S. Ji, F. Liu, H. Wang, X. Wang, Q. Wang, B. Pollet, R. Wang, Highly efficient and stable catalyst based on $Co(OH)_2$@Ni electroplated on Cu-metallized cotton textile for water splitting, ACS Appl. Mater. Inter. 11 (2019) 29791–29798.
[6] R. Wang, Z. Wang, S. Ji, X. Wang, H. Wang, P. Zhou, S. Huo, V. Linkov, A high Faraday efficiency $NiMoO_4$ nanosheet arrays catalyst by adjusting the hydrophilicity for overall water splitting, Chem. Eur J. 26 (2020) 1–9.

[7] H. Wang, Z. Wang, S. Ji, X. Wang, B.G. Pollet, R. Wang, Multidimensional regulation of Ni_3S_2@$Co(OH)_2$ catalyst with high performance for wind energy electrolytic water, J. Power Sources 446 (2020) 227348.

[8] M. Stevens, L. Enman, A. Batchellor, M. Cosby, A. Vise, C. Trang, S. Boettcher, Measurement techniques for the study of thin film heterogeneous water oxidation electrocatalysts, Chem. Mater. 29 (2016) 120–140.

[9] S. Peng, F. Gong, L. Li, D. Yu, D. Ji, T. Zhang, Z. Hu, Z. Zhang, S. Chou, Y. Du, S. Ramakrishna, Necklace-like multishelled hollow spinel oxides with oxygen vacancies for efficient water electrolysis, J. Am. Chem. Soc. 140 (2018) 13644–13653.

[10] N. Cheng, Q. Liu, J. Tian, X. Sun, Y. He, S. Zhai, A.M. Asiri, Nickel oxide nanosheets array grown on carbon cloth as a high-performance three-dimensional oxygen evolution electrode, Int. J. Hydrogen Energy 40 (2015) 9866–9871.

[11] L. Qin, R. Ding, H. Wang, J. Wu, C. Wang, C. Zhang, Y. Xu, L. Wang, B. Lv, Facile synthesis of porous nitrogen-doped holey graphene as an efficient metal-free catalyst for the oxygen reduction reaction, Nano Res. 10 (2016) 305–319.

[12] M. Xiao, Y. Miao, Y. Tian, Y. Yan, Synthesizing nanoparticles of Co-P-Se compounds as electrocatalysts for the hydrogen evolution reaction, Electrochim. Acta 165 (2015) 206–210.

[13] J. Ding, S. Ji, H. Wang, B. Pollet, R. Wang, Mesoporous CoS/N-doped carbon as HER and ORR bifunctional electrocatalyst for water electrolysers and zinc-air batteries, ChemCatChem 11 (2019) 1026–1032.

[14] Y. Zhao, B. Jin, A. Vasileff, Y. Jiao, S. Qiao, Interfacial nickel nitride/sulfide as a bifunctional electrode for highly efficient overall water/seawater electrolysis, J. Mater. Chem. 7 (2019) 8117–8121.

[15] Y. Zhu, Q. Zong, Q. Zhang, H. Yang, Q. Wang, H. Wang, Three-dimensional core-shell NiCoP@NiCoP array on carbon cloth for high performance flexible asymmetric supercapacitor, Electrochim. Acta 299 (2019) 441–450.

[16] G. An, Y. Lee, H. Ahn, Multi-active sites of iron carbide nanoparticles on nitrogen@cobalt-doped carbon for a highly efficient oxygen reduction reaction, J. Alloys Compd. 746 (2018) 177–184.

[17] Y. Liu, X. Xu, P. Sun, T. Chen, N-doped porous carbon nanosheets with embedded iron carbide nanoparticles for oxygen reduction reaction in acidic media, Int. J. Hydrogen Energy 40 (2015) 4531–4539.

[18] K. Raju, K. Ozoemena, Hierarchical one-dimensional ammonium nickel phosphate microrods for high-performance pseudocapacitors, Sci. Rep. 5 (2015) 17629.

[19] Z. Wang, H. Wang, S. Ji, X. Wang, P. Zhou, S. Huo, V. Linkov, R. Wang, Hollow-structured NiCoP nanorods as high-performance electrodes for asymmetric supercapacitors, Mater. Des. 193 (2020) 108807.

[20] Z. Wang, L. Zhou, X.W. Lou, Metal oxide hollow nanostructures for lithium-ion batteries, Adv. Mater. 24 (2012) 1903–1911.

[21] X. Yu, L. Yu, X. Lou, Metal sulfide hollow nanostructures for electrochemical energy storage, Adv. Energy Mater. 6 (2016) 1501333.

[22] X. Wang, J. Feng, Y. Bai, Q. Zhang, Y. Yin, Synthesis, properties, and applications of hollow micro-/nanostructures, Chem. Rev. 116 (2016) 10983–11060.

[23] L. Yu, H. Wu, X. Lou, Self-templated formation of hollow structures for electrochemical energy applications, Acc. Chem. Res. 50 (2017) 293–301.

[24] L. Yu, X.Y. Yu, X.W.D. Lou, The design and synthesis of hollow micro-/nanostructures: present and future trends, Adv. Mater. 30 (2018) 1800939.

[25] H. Wang, X. Shi, S. Ji, X. Wang, L. Zhang, H. Liang, D.J.L. Brett, X. Wang, R. Wang, Tailoring hollow structure within NiCoP nanowire arrays via nanoscale Kirkendall diffusion to enhance hydrogen evolution reaction, Nanotechnology 31 (2020) 425404.

[26] R. Fei, H. Wang, Q. Wang, R. Qiu, S. Tang, R. Wang, B. He, Y. Gong, H.J. Fan, In situ hard-template synthesis of hollow bowl-like carbon: a potential versatile platform for sodium and zinc ion capacitors, Adv. Energy Mater. 10 (2020) 2002741.

[27] F. Lyu, Y. Bai, Z. Li, W. Xu, Q. Wang, J. Mao, L. Wang, X. Zhang, Y. Yin, Self-templated fabrication of CoO-MoO_2 nanocages for enhanced oxygen evolution, Adv. Funct. Mater. 27 (2017) 1702324.

[28] J. Wang, Y. Cui, D. Wang, Design of hollow nanostructures for energy storage, conversion and production, Adv. Mater. 31 (38) (2019) 1801993.

[29] Z. Wang, Z. Wang, H. Wu, X. Lou, Mesoporous single-crystal $CoSn(OH)_6$ hollow structures with multilevel interiors, Sci. Rep. 3 (2013) 1391.

[30] C. Avci, J. Soriano, A. Sanchez, V. Guillerm, C. Carbonell, I. Imaz, D. Maspoch, Post-synthetic anisotropic wet-chemical etching of colloidal sodalite ZIF crystals, Angew. Chem. Int. Edit. 54 (2015) 14417–14421.

[31] Y. Wu, H. Wang, S. Ji, B. Pollet, X. Wang, R. Wang, Engineered porous Ni_2P-nanoparticle/Ni_2P-nanosheet arrays via the Kirkendall effect and Ostwald ripening towards efficient overall water splitting, Nano Res. 13 (2020) 2098–2105.

[32] A. Pan, H.B. Wu, L. Yu, X.W. Lou, Template-free synthesis of VO_2 hollow microspheres with various interiors and their conversion into V_2O_5 for lithium-ion batteries, Angew. Chem. Int. Edit. 52 (2013) 2226–2230.

[33] Y. Chen, L. Yu, X.W. Lou, Hierarchical tubular structures composed of Co_3O_4 hollow nanoparticles and carbon nanotubes for lithium storage, Angew. Chem. Int. Edit. 55 (2016) 5990–5993.

[34] Z. Wang, J. Lu, S. Ji, H. Wang, X. Wang, B. Pollet, R. Wang, Integrating Ni nanoparticles into Mon nanosheets form Schottky heterojunctions to boost its electrochemical performance for water electrolysis, J. Alloys Compd. 867 (2021) 158983.

[35] J. Feng, Y. Yin, Self-templating approaches to hollow nanostructures, Adv. Mater. 31 (2019) 1802349.

[36] S. Peng, L. Li, H.B. Wu, S. Madhavi, X. Lou, Controlled growth of $NiMoO_4$ nanosheet and nanorod arrays on various conductive substrates as advanced electrodes for asymmetric supercapacitors, Adv. Energy Mater. 5 (2015) 1401172.

[37] X. Yu, T. Hua, X. Liu, Z. Yan, P. Xu, P. Du, Nickel-based thin film on multiwalled carbon nanotubes as an efficient bifunctional electrocatalyst for water splitting, ACS Appl. Mater. Inter. 6 (2014) 15395–15402.

[38] L. Wang, X. Wang, P. Kannan, S. Ji, Z. Wang, A highly-stable flexible electrode based on $Co(OH)_2$@$NiSe_2$ electroplated on metals co-coated textiles, Mater. Lett. 279 (2020) 128492.

[39] D. Fa, B. Yu, Y. Miao, Synthesis of ultra-long nanowires of nickel phosphate by a template-free hydrothermal method for electrocatalytic oxidation of glucose, Colloid. Surface. 564 (2019) 31–38.

[40] D. Fa, Y. Miao, Synthesis of $NiHPO_4$–$Ni(OH)_2$ nanowire-assembled bouquets for electrocatalytic oxidation of methanol and urea, J. Appl. Electrochem. 50 (2020) 1091–1099.

[41] Y. Wu, S. Ji, H. Wang, B. Pollet, X. Wang, R. Wang, A highly efficient water electrolyser cell assembled by asymmetric array electrodes based on Co, Fe-doped $Ni(OH)_2$ nanosheets, Appl. Surf. Sci. 528 (2020) 146972.

[42] H. Wu, T. Zhu, X. Lu, G.W. Ho, High-efficient electrocatalysts by unconventional acid-etching for overall water splitting, J. Mater. Chem. 5 (2017) 24153–24158.

[43] H. Zhang, G. Shen, X. Liu, B. Ning, C. Shi, L. Pan, X. Zhang, Z. Huang, J. Zou, Self-supporting NiFe LDH-MoS integrated electrode for highly efficient water splitting at the industrial electrolysis conditions, Chin. J. Catal. 42 (2021) 1732–1741.

[44] S. Ahn, B. Lee, I. Choi, S. Yoo, H. Kim, E. Cho, D. Henkensmeier, S.W. Nam, S.-K. Kim, J.H. Jang, Development of a membrane electrode assembly for alkaline water electrolysis by direct electrodeposition of nickel on carbon papers, Appl. Catal. B Environ. 154–155 (2014) 197–205.